

## Anisotropic flows and dihadron correlations in heavy ion collisions

---

**Che-Ming Ko**<sup>\*†</sup>

*Cyclotron Institute and Department of Physics and Astronomy, Texas A&M University, college Station, Texas 77843-3366, USA*

*E-mail: ko@comp.tamu.edu*

**Jun Xu**

*Department of Physics and Astronomy, Texas A&M University-Commerce, Commerce, Texas 75429-3011, USA*

*E-mail: Jun\_Xu@tamu-commerce.edu*

Using a multiphase transport model that includes both initial partonic and final hadronic scatterings, we have studied anisotropic flows and dihadron correlations as functions of pseudorapidity and azimuthal angular differences between trigger and associated particles in heavy ion collisions at LHC. With parameters in the model determined from fitting the measured multiplicity density of mid-pseudorapidity charged particles in central collisions and their elliptic flow in mid-central collisions, the calculated higher-order anisotropic flows from the two-particle cumulant method reproduce approximately those measured in experiments. Similar to experimental results, the two-dimensional dihadron correlations at most central collisions show a ridge structure at the near side and a broad structure at the away side. The short- and long-range dihadron azimuthal correlations, corresponding to small and large pseudorapidity differences, respectively, are studied for triggering particles with different transverse momenta and are found to be qualitatively consistent with experimental results.

*The Seventh Workshop on Particle Correlations and Femtoscopy  
September 20 - 24 2011  
University of Tokyo, Japan*

---

<sup>\*</sup>Speaker.

<sup>†</sup>Based on work supported by the U.S. National Science Foundation under Grant Nos. PHY-0758115 and PHY-1068572, the US Department of Energy under Contract No. DE-FG02-10ER41682, and the Welch Foundation under Grant No. A-1358.

## 1. Introduction

Recently, results from the first Pb-Pb collisions at  $\sqrt{s_{NN}} = 2.76$  TeV at the Large Hadron Collider (LHC) have attracted a lot of attentions [1, 2, 3, 4]. In the most central collisions (0 – 5%), the multiplicity density of produced charged particles at mid-pseudorapidity is about 2.2 times of that in Au+Au collisions at  $\sqrt{s_{NN}} = 200$  GeV at RHIC. The measured elliptic flow is, on the other hand, of a similar magnitude as that measured at RHIC. Besides, experimental data on higher-order flows [5] and dihadron correlations [6] have also become available. Furthermore, it was found that the long-range dihadron azimuthal correlations could be entirely accounted for by the anisotropic flows [5, 6]. To understand these results, we have carried out a study using a multiphase transport (AMPT) model [7] that uses the heavy ion jet interaction generator (HIJING) model [8] to generate the initial particle distributions. In the version of string melting, all hadrons produced in the HIJING model through Lund string fragmentation are converted to their valence quarks and antiquarks, whose evolution in time and space is modeled by Zhang’s parton cascade (ZPC) model [9]. After their scatterings, quarks and antiquarks are converted via a spatial coalescence model to hadrons, and the scatterings among them are described by a relativistic transport (ART) model [10]. With parameters in the model determined from fitting the measured multiplicity density of mid-pseudorapidity charged particles in central collisions and their elliptic flow in mid-central collisions at LHC [11], we then studied the dependence of the anisotropic flows and dihadron correlations on the pseudorapidity and azimuthal angular difference between trigger and associated particles in these collisions [12].

## 2. Anisotropic flows

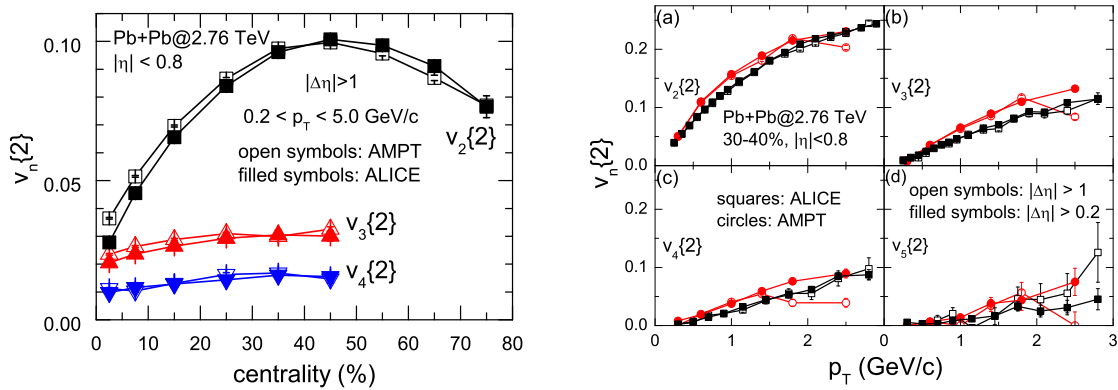


**Figure 1:** Left window: Centrality dependence of  $v_n$  ( $n = 2, 3, 4$ ) for mid-pseudorapidity ( $|\eta| < 0.8$ ) charged particles obtained from the two-particle cumulant method in Pb-Pb collisions at  $\sqrt{s_{NN}} = 2.76$  TeV from the string melting AMPT model. Right window: Transverse momentum dependence of  $v_2$  (a),  $v_3$  (b),  $v_4$  (c), and  $v_5$  (d) in same collisions at 30 – 40% centralities. The ALICE data (squares) are taken from Ref. [5]. Results for  $|\Delta\eta| > 0.2$  and  $|\Delta\eta| > 1$  are shown by filled and open symbols, respectively.

We first show in the left window of Fig. 1 by open symbols the centrality dependence of transverse-momentum-integrated ( $0.2 < p_T < 5.0$  GeV/c) anisotropic flows  $v_n$  ( $n = 2, 3, 4$ ) for mid-pseudorapidity charged particles in Pb-Pb collisions at  $\sqrt{s_{NN}} = 2.76$  TeV from the AMPT model. They are calculated with the two-particle cumulant method ( $v_n = \sqrt{\langle \cos(n\Delta\phi) \rangle}$ ) from particle pairs with pseudorapidity difference  $|\Delta\eta| > 1$  as in experimental analysis [5] to reduce the nonflow effect. Compared with the ALICE data (filled symbols) [5], the AMPT model reproduces reasonably well the centrality dependence of  $v_n$  ( $n = 2, 3, 4$ ). In the right window of Fig. 1, we display by circles the transverse momentum dependence of anisotropic flows  $v_n$  ( $n = 2, 3, 4, 5$ ) of mid-pseudorapidity ( $|\eta| < 0.8$ ) charged particles in the mid-central (30–40%) collisions and compare them with the ALICE data (squares) from Ref. [5]. It is seen that the anisotropic flows for different pseudorapidity cut  $|\Delta\eta| > 0.2$  and  $|\Delta\eta| > 1$  are similar to those from the ALICE data, while at larger transverse momenta in the case of the smaller pseudorapidity cut the AMPT model gives larger values due to overestimated nonflow effects. We note that as for RHIC [13], anisotropic flows for the most central collisions from the AMPT model are overestimated in comparison with those from the ALICE data as a result of the constant parton scattering cross section used in the AMPT model for all centralities. Using a medium-dependent parton scattering cross section is expected to lead to a better description of the data. It is worthwhile to point out that once the elliptic flow is fitted in the AMPT model, the higher-order flows are automatically consistent with the experimental data, thus indicating that the HIJING model, as an initial distribution generator, provides the correct initial spatial anisotropies through the Glauber model calculation.

### 3. Dihadron correlations

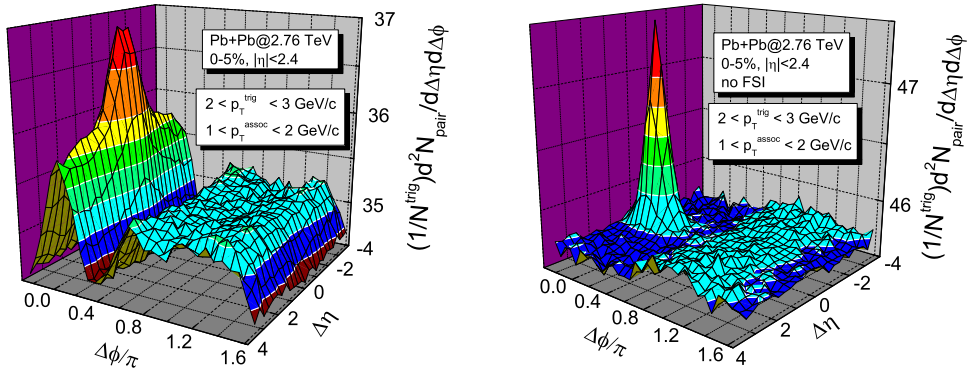


**Figure 2:** Two-dimensional dihadron correlation per trigger particle as a function of  $\Delta\eta$  and  $\Delta\phi$  for  $1 < p_T^{\text{assoc}} < 2$  GeV/c and  $2 < p_T^{\text{trig}} < 3$  GeV/c in the most central (0–5%) Pb-Pb collisions at  $\sqrt{s_{NN}} = 2.76$  TeV from the string melting AMPT model with (left window) and without (right window) final-state interactions (FSI).

In the left window of Fig. 2, we show the two-dimensional dihadron correlation per trigger particle from the string melting AMPT model in the 0–5% most central Pb-Pb collisions at

$\sqrt{s_{NN}} = 2.76$  TeV for trigger particles and associated particles in the transverse momentum windows  $2 < p_T^{\text{trig}} < 3$  GeV/c and  $1 < p_T^{\text{assoc}} < 2$  GeV/c, respectively. It is calculated according to  $(1/N^{\text{trig}})d^2N_{\text{pair}}/d\Delta\eta d\Delta\phi = B(0,0)S(\Delta\eta, \Delta\phi)/B(\Delta\eta, \Delta\phi)$  [6], where  $S(\Delta\eta, \Delta\phi)$  is the raw correlation per trigger particle from pairs in same events and  $B(\Delta\eta, \Delta\phi)$  is the background correlation per trigger particle from pairs in different events, and  $B(\Delta\eta = 0, \Delta\phi = 0)$  is the normalization factor. Similar to the experimental results in Ref. [6], there is a peak at  $\Delta\eta = 0$  and a ridge structure extending to  $|\Delta\eta| = 4$  at the near side ( $\Delta\phi \sim 0$ ) as well as a broad structure at the away side which also extends to  $|\Delta\eta| = 4$ . There have been many explanations for the ridge structure in dihadron correlations [14, 15, 16, 17, 18, 19, 20]. As in Refs. [5, 6, 21], the ridge structure seen in AMPT mainly comes from the anisotropic flows. To illustrate this effect, we have repeated the calculation by turning off both partonic and hadronic scatterings in the AMPT model, and the results are shown in the right window of Fig. 2. It is seen that the near-side ridge now disappears and the away-side broad structure is also largely weakened as both are results of the collective flow that is generated by final-state interactions (FSI). Furthermore, the peak along the  $\Delta\eta$  direction is sharper than that in the case with FSI.

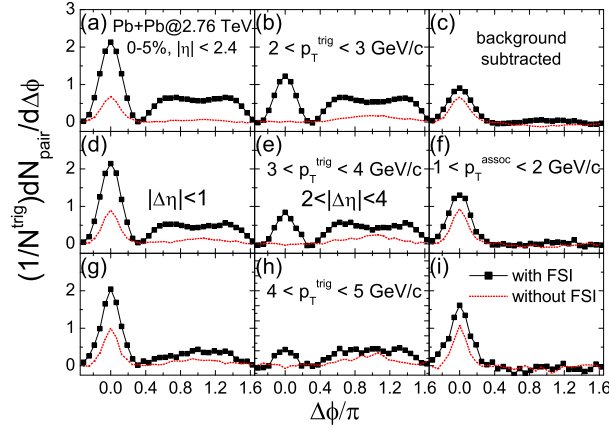


**Figure 3:** Short-range ( $|\Delta\eta| < 1$ , (a), (d) and (g)) and long-range ( $2 < |\Delta\eta| < 4$ , (b), (e) and (h)) dihadron correlations per trigger particle as functions of the azimuthal angular difference  $\Delta\phi$  for different transverse momentum windows of trigger particles from 0 – 5% most central Pb-Pb collisions in the string melting AMPT model with (solid lines) and without (dashed lines) final-state interactions. The difference between the short-range and long-range dihadron azimuthal correlation is shown in panels (c), (f), and (i).

Left and middle columns of Fig. 3 show, respectively, the short-range ( $|\Delta\eta| < 1$ ) and long-range ( $2 < |\Delta\eta| < 4$ ) dihadron azimuthal angular correlations, obtained by taking average of the two-dimensional dihadron correlation over the corresponding  $\Delta\eta$  windows [6], for different transverse momenta of trigger particles. Compared with the short-range correlations, the long-range correlations have much weaker peaks at the near side due to the absence of the nonflow contribution, resulting in a smaller yield of near-sided associated particles. Also, the strength of near-side correlations decreases with increasing  $p_T$  of trigger particles for both short- and long-range correlations. As a result, the near-side associated yield in the jet region, given by the difference between the associated yields in the long-range correlation and the short-range correlation, increases with

increasing  $p_T$  of trigger particles. This is in contrary to the decreasing near-side associated yield in the ridge region, defined by the long-range correlation, with increasing  $p_T$  of trigger particles. For the strength of away-side correlations, it decreases, on the other hand, with increasing  $p_T$  of trigger particles for both short-range and long-range correlations.

Since the long-range dihadron correlation is largely caused by the anisotropic flows and their fluctuations [5, 6, 21], dihadron correlations due to the back-to-back jet pairs produced in initial hard collisions can be estimated by subtracting the long-range correlations from the short-range correlations, and the resulting background subtracted correlations are shown in the right column of Fig. 3. It is seen that the away-side correlations are now very weak for all cases, similar to the results of Refs. [22, 23], in which the background correlations are obtained from replacing the event average of products with the product of averages in the approximate correlations calculated with the Fourier expanded particle azimuthal distributions. Also, the near-side correlations are stronger for higher- $p_T$  trigger particles as a result of the stronger medium response to higher- $p_T$  jets. For comparisons, we also show in Fig. 3 by dashed lines the dihadron azimuthal correlations obtained without final-state interactions, which are similar to those from p+p collisions at the same energy. The background-subtracted away-side correlations in this case is similar to that obtained with final-state interactions. The smearing of the away-side jet in heavy ion collisions without final-state interactions or p+p collisions is due to the fairly low  $p_T$  of trigger and associated particles considered here, which can lead to an away-side jet with very different pseudorapidity from that of the triggered jet [24] as shown in the middle column of Fig. 3. A peak in the away-side correlations of such collisions would, however, appear if the associated particles have similar momenta as those of the trigger particles or the trigger particles have very high  $p_T$ . This is very different from the case where final-state interactions are included. Because of jet quenching as a result of final-state interactions, no peak structure is seen in the away-side correlations unless the trigger particles have extremely high  $p_T$ .

#### 4. Conclusions and discussions

We have studied anisotropic flows and dihadron correlations in Pb-Pb collisions at  $\sqrt{s_{NN}} = 2.76$  TeV within a multiphase transport model with parameters fitted to reproduce the measured multiplicity density of mid-pseudorapidity charged particles in central collisions and their elliptic flow in mid-central collisions. We have found that the resulting higher-order anisotropic flows slightly overestimate the experimental data at small centralities but are consistent with them at other centralities. We have obtained the ridge structure along the pseudorapidity direction in the near side of the dihadron correlations, and it disappears when final-state interactions are turned off in our model. We have also studied both the short-range and long-range dihadron azimuthal correlations for different transverse momenta of trigger particles, and they are seen to be quantitatively consistent with experimental results. We have further attempted to determine the background-subtracted short-range dihadron azimuthal correlations by taking the long-range dihadron azimuthal correlations as the background, and they are found to be similar to those obtained previously using a different method.

It is of interest to mention that because of the constant parton scattering cross section used in the AMP model, the specific viscosity of the initial partonic matter in this model is about 0.37,

which is about a factor of two larger than the values extracted with the viscous hydrodynamic model [25, 26]. Including the temperature dependence of the local screening mass in the evaluation of the parton scattering cross section in the AMPT model as in Ref. [27] may help to better understand the different results from the transport model and the hydrodynamic model.

## References

- [1] K. Aamodt *et al.* (ALICE Collaboration), Phys. Rev. Lett. **105**, 252301 (2010).
- [2] K. Aamodt *et al.* (ALICE Collaboration), Phys. Rev. Lett. **105**, 252302 (2010).
- [3] K. Aamodt *et al.* (ALICE Collaboration), Phys. Rev. Lett. **106**, 032301 (2011).
- [4] K. Aamodt *et al.* (ALICE Collaboration), Phys. Lett. **B696**, 30 (2011).
- [5] K. Aamodt *et al.* (ALICE Collaboration), Phys. Rev. Lett. **107**, 032301 (2011).
- [6] S. Chatrchyan *et al.* (CMS Collaboration), arXiv:1105.2438 [nucl-ex].
- [7] Z.W. Lin, C.M. Ko, B.A. Li, B. Zhang, and S. Pal, Phys. Rev. C **72**, 064901 (2005).
- [8] X.N. Wang and M. Gyulassy, Phys. Rev. D **44**, 3501 (1991).
- [9] B. Zhang, Comput. Phys. Commun. **109**, 193 (1998).
- [10] B. A. Li and C.M. Ko, Phys. Rev. C **52**, 2037 (1995).
- [11] J. Xu and C.M. Ko, Phys. Rev. C **83**, 034904 (2011).
- [12] J. Xu and C.M. Ko, Phys. Rev. C **84**, 044907 (2011).
- [13] J. Xu and C.M. Ko, Phys. Rev. C **83**, 021903 (2011).
- [14] N. Armesto, C.A. Salgado, and U.A. Wiedemann, Phys. Rev. Lett. **93**, 242301 (2004).
- [15] L.M. Satarov, H. Stöcker, and I.N. Mishustin, Phys. Lett. **B627**, 64 (2005).
- [16] C.B. Chiu and R.C. Hwa, Phys. Rev. C **72**, 034903 (2005).
- [17] C.Y. Wong, Phys. Rev. C **76**, 054908 (2007).
- [18] P. Romatschke, Phys. Rev. C **75**, 014901 (2007).
- [19] A. Majumder, B. Müller, and S.A. Bass, Phys. Rev. Lett. **99**, 042301 (2007).
- [20] E. Shuryak, Phys. Rev. C **76**, 047901 (2007).
- [21] M. Luzum, Phys. Lett. **B696**, 499 (2011).
- [22] J. Xu and C.M. Ko, Phys. Rev. C **84**, 014903 (2011).
- [23] G.L. Ma and X.N. Wang, Phys. Rev. Lett. **106**, 162301 (2011).
- [24] X.N. Wang, Phys. Rep. **280**, 287 (1997).
- [25] H Song, S. Bass, and U. Heinz, Phys. Rev. C **83**, 054912 (2011).
- [26] B. Schenke, S. Jeon, and C. Gale, Phys. Rev. Lett. **106**, 042301 (2011).
- [27] B. Zhang and W.A. Wortman, Phys. Lett. **B693**, 24 (2010).